

Continuous-variable entanglement distillation over a pure loss channel with multiple quantum scissors

Kaushik P. Seshadreesan¹, Hari Krovi², and Saikat Guha¹

¹*College of Optical Sciences, University of Arizona, Tucson, AZ 85721, USA*

²*Quantum Engineering and Computing Physical Sciences and Systems,*

Raytheon BBN Technologies, Cambridge, MA 02138, USA

(Dated: June 21, 2019)

Entanglement distillation is a key primitive for distributing high quality entanglement between remote locations. Probabilistic noiseless linear amplification based on the quantum scissors is a candidate for entanglement distillation from noisy continuous-variable (CV) entangled states. Being a non-Gaussian operation, the quantum scissors is challenging to analyze. We present a derivation of the non-Gaussian state heralded by multiple quantum scissors in a pure loss channel with two-mode squeezed vacuum input. We choose the reverse coherent information (RCI)—a proven lower bound on the distillable entanglement of a quantum state under one-way local operations and classical communication (LOCC), as our figure of merit. We evaluate a Gaussian lower bound on the RCI of the heralded state. We show that it can exceed the unlimited two-way LOCC-assisted direct transmission entanglement distillation capacity of the pure loss channel. The optimal heralded Gaussian RCI with two quantum scissors is found to be significantly more than that with a single quantum scissors, albeit at the cost of decreased success probability. Our results fortify the possibility of a quantum repeater scheme for CV quantum states using the quantum scissors.

I. INTRODUCTION

Entanglement shared across large distances is a key resource for quantum information processing tasks such as distributed quantum computation [1–3], distributed sensing [4–6], quantum communication protocols such as quantum key distribution [7], quantum teleportation [8], superdense coding [9], entanglement assisted high rate quantum error correcting codes [10], and entanglement-assisted classical communication over noisy channels [11].

Optical photons are arguably the best carriers of quantum information to distribute entanglement between remote locations [12]. Optical entanglement distribution is largely classified into schemes based on discrete and continuous variables (DV and CV) depending on the entangled resource state that is transmitted [13, 14]. In DV, the resource states are maximally entangled states of discrete, finite-dimensional degrees of freedom of single photons, such as the polarization; while in CV, they are entangled multimode squeezed states of the continuous, infinite-dimensional, quadrature degrees of freedom of electromagnetic field modes, which are Gaussian states, i.e., states completely described by the first two moments of the quadrature operators associated with the modes.

The primary challenge in distributing optical entanglement is photon loss and noise in transmission, which degrades the quality of entanglement. Thus, entanglement distillation—the process of distilling from several copies of a noisy entangled state fewer copies of a more entangled state using local operations and classical communication (LOCC), is key in distributing high quality entanglement. Entanglement distillation in DV, e.g., from weakly entangled mixed states of pairs of single-photon polarization qubits, typically involves the quantum CNOT gate [15, 16], or more practically, a simple polarizing beam splitter [17], acting locally on pairs of

identical copies of the state, followed by measurement and classical communication between the two parties. When applied recursively, they yield highly entangled and highly pure two-qubit states [18]. In CV, it is known that entanglement distillation from noisy Gaussian entangled states cannot be effected by Gaussian operations alone [19, 20], where the latter refer to state transformations based on Hamiltonians that are at most quadratic in the quadrature operators and map Gaussian states to other Gaussian states. Non-Gaussian operations such as photon counting are required. In this regard, schemes based on Fock state filtering [21], such as quantum catalysis [22, 23], photon subtraction [24, 25], symmetric photon replacement [26–28] and purifying distillation [29], which degaussify Gaussian states, have been considered. When applied recursively, these schemes regaussify the final output while yielding highly entangled [25, 26], and in some cases also highly pure Gaussian states [28, 29].

In Ref. [30], Ralph and Lund proposed the concept of probabilistic noiseless linear amplification (NLA), which can be realized using the non-Gaussian operation—the quantum scissors [31], as a candidate for CV entanglement distillation. In the limit of a large number of scissors, NLA can probabilistically distill highly entangled and highly pure Gaussian states from weakly entangled, mixed Gaussian states [30]. Approximate NLA based on a single quantum scissors was further investigated in [32, 33] for quantum error correction [34] of CV entangled states, towards designing quantum repeaters [35–37]. CV entanglement distillation with a single quantum scissors was experimentally demonstrated in [38].

In this paper, we analyze entanglement distillation with approximate NLA effected by multiple, but finite number of quantum scissors over a pure loss channel with two-mode squeezed vacuum state (TMSV) input. We show that the entanglement content of the heralded

output of the NLA—quantified by the *reverse coherent information* (RCI) [39–42]—is higher than

$$C_{\text{direct}}(\eta) = -\log(1 - \eta), \quad (1)$$

the recently proven maximum entanglement generation rate in ebits (maximally entangled qubits) per mode achievable through a pure-loss channel of transmissivity η [40, 43] (see also [44] for a strong converse theorem.) The RCI is an information-theoretic lower bound on the distillable entanglement per copy of a shared state that is achievable using one-way LOCC when many copies of the shared state are available [43, 45]. Although NLA has been proposed in the past for CV entanglement distillation, this is the first time the optimal trade-off between the RCI of the heralded state and the probability of success of the NLA as a function of the scissor-based NLA’s internal parameters, a gain (transmissivity of a beamsplitter) and the number of scissors is quantified. Clearly, RCI times the NLA success probability must be less than $C_{\text{direct}}(\eta)$ [43]. But, being able to herald entanglement over a lossy channel, even if probabilistically, of RCI higher than $C_{\text{direct}}(\eta)$, i.e., heralding a state of distillable entanglement higher than $C_{\text{direct}}(\eta)$, is significant towards realizing CV quantum repeaters since the latter is a pre-requisite to building a second-generation quantum repeater that can outperform $C_{\text{direct}}(\eta)$ [46].

More technically, the contributions of this paper include a calculation of the non-Gaussian state heralded by the approximate NLA based on multiple but finite number of quantum scissors and the corresponding heralding success probability, based on characteristic functions and the Husimi Q function. The calculation also applies to the teleportation-based CV error correction scheme with approximate NLA [34], and is computationally efficient. This is in contrast to the Fock basis calculations presented in [32, 33], which do not scale well with increasing number of quantum scissors. Our choice of the RCI as the figure of merit is operationally more relevant than those considered before, such as the logarithmic negativity [47, 48] and the entanglement of formation (EOF) [49]. We numerically evaluate a Gaussian lower bound on the RCI of the state heralded by approximate NLA. We show that there exist TMSV input mean photon numbers and scissors gain parameter values where the lower bound exceeds $C_{\text{direct}}(\eta)$. Further, we find that the Gaussian RCI heralded by two quantum scissors is significantly higher compared to that heralded by a single quantum scissors, and in some cases the addition of the second quantum scissors even helps boost it above $C_{\text{direct}}(\eta)$, which could not be achieved with just a single quantum scissors. In addition to the analyses based on the RCI, we also evaluate a Gaussian lower bound on the EOF of the state heralded by a single quantum scissors. We qualitatively validate the findings presented in [33] and extend the analysis to two quantum scissors.

The paper is organized as follows. In Sec. II, we review the basic concept of NLA with quantum scissors, outlining its relevance to CV entanglement distillation.

In Sec. III, we describe in detail the methods we employ to analyze CV entanglement distillation using multiple, but finite number of quantum scissors, including our figure of merit the RCI. Section IV contains the results. Finally, we summarize our findings in Sec. V.

II. NOISELESS LINEAR AMPLIFICATION WITH QUANTUM SCISSORS

Noiseless linear amplification [30] refers to probabilistic amplification that, e.g., transforms coherent states as $|\alpha\rangle \rightarrow |g\alpha\rangle$ where $g \in \mathbb{R}$ is the gain. NLA can be implemented in a heralded fashion using linear optics, photon injection and detection [30]. The scheme involves splitting the input signal into N parts of equal intensity and recombining them following the quantum scissors operation on each part as shown in Fig. 1 (a).

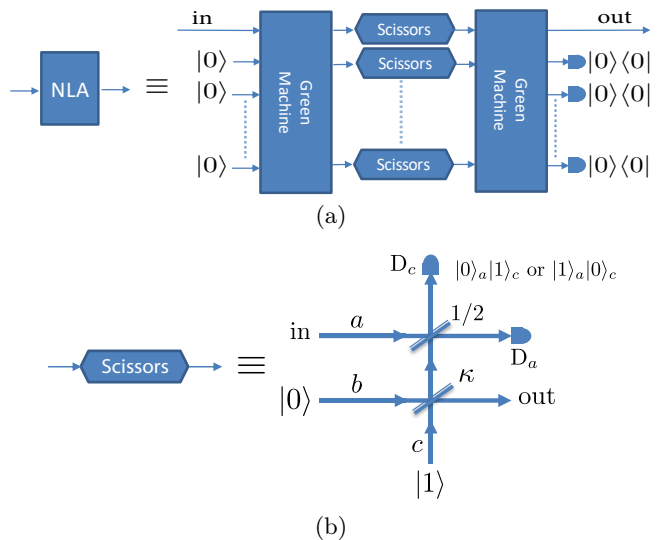


Figure 1. (a) Noiseless linear amplification (NLA) implemented using linear optics and (b) the quantum scissors operation based on photon injection and detection. The Green Machines in (a) refer to an n -mode input n -mode device that performs a n -way splitting or its inverse (recombining) unitary operation. When all but one of the input modes are in the vacuum state, the Green machine splits the mean photon number in the first input mode uniformly across all the output modes.

Quantum scissors, as the name suggests, refers to an operation that truncates a quantum state in Fock space [31]. In addition to truncation, it can be used to amplify certain Fock state components of the state relative to others [30]. Consider the scheme shown in Fig. 1 (b) comprising of single photon injection and detection. A single photon (in mode c) is mixed with vacuum (in mode b) on a beam splitter of transmissivity $\kappa = 1/(1 + g^2)$ (g being the intended gain of NLA), creating an entangled state in the $\{|0\rangle_b \otimes |1\rangle_c, |1\rangle_c \otimes |0\rangle_b\}$ subspace. When the signal in mode a is mixed with

mode c on a 50:50 beam splitter and either one of the two projections $\{|0\rangle_a \otimes |1\rangle_c, |1\rangle_a \otimes |0\rangle_c\}$ is applied (i.e., when detector D_a clicks and D_c doesn't, or vice versa), the $\{|0\rangle, |1\rangle\}$ support of the quantum state of the signal is teleported to mode b . Further, the teleported state is such that its $|1\rangle$ component is amplified relative to the vacuum component depending on the choice of κ . In summary, the quantum scissors scheme of Fig. 1 on any input signal state $|\psi\rangle \propto \alpha_0 |0\rangle + \alpha_1 |1\rangle + \dots$ heralds the truncated and amplified output

$$\Gamma(g) (\alpha_0 |0\rangle + \alpha_1 |1\rangle + \dots) = \sqrt{\frac{1}{1+g^2}} (\alpha_0 |0\rangle + g\alpha_1 |1\rangle). \quad (2)$$

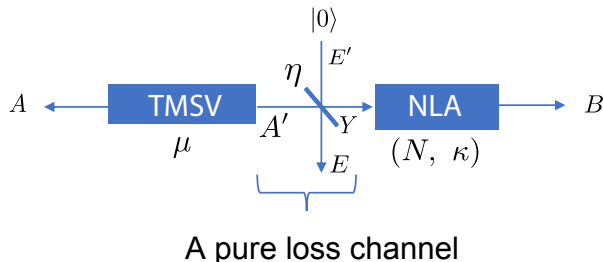


Figure 2. A pure loss channel of transmissivity η with TMSV state input appended by N -quantum scissors of gain $g = \sqrt{(1-\kappa)/\kappa}$ at the output.

When the signal to the modified quantum scissors is sufficiently weak such that its quantum state resides primarily in the $\{|0\rangle, |1\rangle\}$ subspace, the operation effects NLA; whereas if the state has significant support on higher photon components, then the amplification is not noiseless anymore owing to the excess noise originating from the truncation of the teleported state in Fock space. Thus, in the scheme of Fig. 1 (a), for a given input signal intensity, N needs to be sufficiently large so that the sub-signals that are inputs to the quantum scissors operations are weak. When all the quantum scissors operations succeed and all-but-one of the outputs of the N -combiner are measured in the vacuum state, the device approaches NLA.

As mentioned earlier, NLA is probabilistic. The success probability of NLA with N -quantum scissors is input state dependent and decreases exponentially with N . For an input coherent state $|\alpha\rangle$, the success probability of an N -scissors NLA drops with N and the NLA gain g as $P_s = 1/(1+g^2)^N e^{-(1-g^2)|\alpha|^2}$ [30].

NLA is particularly relevant to CV entanglement distillation. Consider a TMSV state of mean photon number $\mu = \sinh^2 r$

$$|\Psi\rangle_{AA'} = \sqrt{1-\chi^2} \sum_{n=0}^{\infty} \chi^n |n\rangle_A \otimes |n\rangle_{A'}, \quad \chi = \tanh r, \quad (3)$$

where r is the squeezing parameter. Let one mode of the TMSV state be transmitted through a pure loss chan-

nel of transmissivity η , followed by N -quantum scissors, as shown in Fig. 2, where N is sufficiently large, so that it implements NLA of gain $g = \sqrt{(1-\kappa)/\kappa}$. The NLA results in a heralded state that is equivalent to the state obtained by transmitting one mode of a TMSV state of higher mean photon number $\mu' = \sinh^2(\tanh^{-1}(\chi\sqrt{1+(g^2-1)\eta}))$ through a pure loss channel of improved transmissivity given by $\eta' = g^2\eta/(1+(g^2-1)\eta)$, as shown in [30], which implies improved entanglement shared across the channel.

III. CV ENTANGLEMENT DISTILLATION WITH MULTIPLE QUANTUM SCISSORS: METHODS

Our analysis of CV entanglement distillation across a pure loss bosonic channel using multiple, but finite N -quantum scissors with TMSV input as shown in Fig. 2 involves the following steps: a) determining the heralded non-Gaussian quantum state, b) determining the heralding success probability, and c) evaluating a figure of merit for the task.

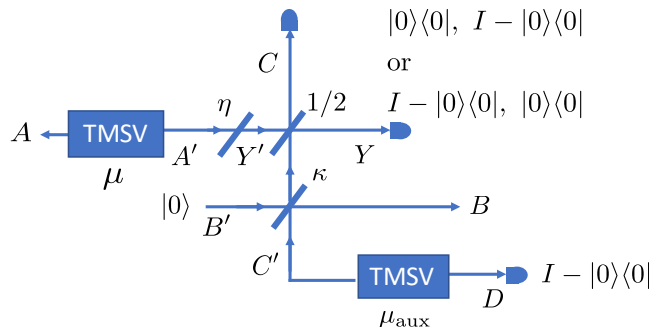


Figure 3. A modified quantum scissors implemented with a weak EPR source and ON-OFF projections, appended to a pure loss channel of transmissivity η with TMSV state input. When the idler mode of the weak TMSV state is projected on $I - |0\rangle\langle 0|$ a single photon is heralded in the signal mode and injected into the quantum scissors.

A. Quantum scissors based on heralded single photon injection and ON-OFF photodetection

The calculation of the non-Gaussian state heralded by N -quantum scissors of the form shown in Fig. 1 (b) quickly becomes cumbersome with increasing (but finite) N (c.f. [32, 33]). In order to make the calculation more tractable, we emulate the quantum scissors by replacing the photon number detectors with ON-OFF photodetection $\{|0\rangle\langle 0|, I - |0\rangle\langle 0|\}$, and the single photon by one mode of a weak TMSV state (of mean photon number μ_{aux}). Figure 3 shows such an emulation of a single-quantum scissors NLA (denoted as $N=1$ -NLA hereafter) acting on a pure loss channel with TMSV input.

The weak TMSV state heralds a single photon state for injection into the quantum scissors when the idler mode is projected onto $I - |0\rangle\langle 0|$. Note that in all the calculations presented in this paper, we choose $\mu_{\text{aux}} = 0.01$. The success probability of the quantum scissors operation is expected to be enhanced having replaced the $\{|0\rangle, |1\rangle\}$ projection with $\{|0\rangle\langle 0|, I - |0\rangle\langle 0|\}$ detection, whereas the quality of the amplification is expected to be marginally degraded. However, the qualitative behavior of the scheme still remains preserved as is shown in subsequent analyses.

B. Heralded state and heralding success probability

We now describe the calculation of the heralded non-Gaussian quantum state and heralding success probability for the scheme shown in Fig. 3. The scheme involves a bosonic system of five modes, whose pre-measurement state is Gaussian, meaning the quantum state is completely described by its first two moments. See Appendix A for the system description, and the initial and pre-measurement covariance matrices. See [50, 51] for a detailed account of CV quantum information including entanglement in CV Gaussian states.

The quantum scissors operation is successful when, in Fig. 3, either one (but not both) of the modes C and Y , along with mode D are measured in the ‘‘ON’’ projection $I - |0\rangle\langle 0|$. The heralded state clearly is non-Gaussian since the $I - |0\rangle\langle 0|$ projection is non-Gaussian. We capture the heralded non-Gaussian state in modes A and B by its Husimi Q function, defined as

$$Q_\rho(\alpha, \beta) = \frac{\langle \alpha, \beta | \rho | \alpha, \beta \rangle}{\pi^2}, \quad \alpha, \beta \in \mathbb{C}. \quad (4)$$

It can be determined as an overlap integral between the five mode Gaussian state ρ in modes $ABCDY$ and the projections $|\alpha\rangle\langle \alpha|_A \otimes |\beta\rangle\langle \beta|_B \otimes (I - |0\rangle\langle 0|)_{CD}^{\otimes 2} \otimes |0\rangle\langle 0|_Y$ or $|\alpha\rangle\langle \alpha|_A \otimes |\beta\rangle\langle \beta|_B \otimes |0\rangle\langle 0|_C \otimes (I - |0\rangle\langle 0|)_{DY}^{\otimes 2}$, normalized by the probability of the projections $\pi_1 = (I - |0\rangle\langle 0|)_{CD}^{\otimes 2} \otimes |0\rangle\langle 0|_Y$ and $\pi_2 = |0\rangle\langle 0|_C \otimes (I - |0\rangle\langle 0|)_{DY}^{\otimes 2}$, respectively, which constitute the success probability of the quantum scissors operation. The heralded states corresponding to the two possible successful projections turn out to be the same up to local phases.

The above overlap integrals are sums of Gaussian integrals that can be evaluated efficiently (Appendix C). For example, the success probability for the projection π_1 on modes CDY involves evaluating the overlap integral $P_1 = \text{Tr}(\pi_1 \rho_{ABCDY})$,

$$P_1 = \int d\xi \chi_{\rho_{ABCDY}}(\xi) (1 - \chi_0(-\xi_C)) \times (1 - \chi_0(-\xi_D)) (\chi_0(-\xi_Y))_Y, \quad \xi \in \mathbb{R}, \quad (5)$$

where $\chi_{\rho_{ABCDY}}$ and $\chi_0 = \chi_{|0\rangle\langle 0|}$ are the characteristic functions of the heralded non-Gaussian state and the vacuum state, respectively. The success probability associated with the other projection, namely π_2 also turn out to be the same as (5) due to symmetry between modes C and Y , so that the total success probability is $P'_{\text{succ}} = \text{Tr}((\pi_1 + \pi_2)\rho) = P_1 + P_2 = 2P_1$. The success probability of a quantum scissors operation with a deterministic single photon injection into mode C can be deduced from the above success probability by renormalizing it with the probability of detecting a single photon in the idler mode D . That is,

$$P_{\text{succ}} = P'_{\text{succ}} / \left(\frac{\mu_{\text{aux}}}{\mu_{\text{aux}} + 1} \right), \quad (6)$$

where the scaling factor is the probability of observing the $|1\rangle\langle 1|$ projection on the idler mode of the TMSV state of mean photon number μ_{aux} .

The heralded state and heralding success probability calculations for NLA with higher number of quantum scissors follow similarly to the $N = 1$ -NLA case described above. For N quantum scissors, the success probability P_{succ} is obtained by renormalizing P'_{succ} by a factor $(\mu_{\text{aux}}/(\mu_{\text{aux}}+1))^N$.

C. Reverse coherent information

The reverse coherent information (RCI) of a state ρ_{AB} is defined as [39–42]

$$I_R(\rho_{AB}) := H(A)_\rho - H(AB)_\rho, \quad (7)$$

where $H(A)_\rho$ is the von Neumann entropy of $\rho_A = \text{Tr}_B(\rho_{AB})$ defined as $H(A)_\rho = -\text{Tr}(\rho_A \log_2 \rho_A)$ (and likewise $H(AB)_\rho$).

For the CV entanglement distillation scheme of Fig. 3, we determine the optimal RCI that can be heralded by numerically optimizing over the mean photon number of the input TMSV state and the NLA gain [52].

D. A lower bound on the heralded reverse coherent information

Evaluating the RCI of the state heralded upon successful operation of quantum scissors-based NLA following the pure loss channel is perceived to be nontrivial. As an interim remedy, we resort to calculating the RCI of the covariance matrix of the heralded state, which by the Gaussian extremality theorem [53] amounts to a lower bound on the RCI of the heralded non-Gaussian state.

The covariance matrix $V(\rho)$ can be determined from the Q function as

$$V_{i,j}(\rho) = 2 \int d\mathbf{r} r_i r_j Q_\rho(\alpha, \beta) - \delta_{i,j} - 2 \int d\mathbf{r} r_i Q_\rho(\alpha, \beta) \int d\mathbf{r} r_j Q_\rho(\alpha, \beta), \quad (8)$$

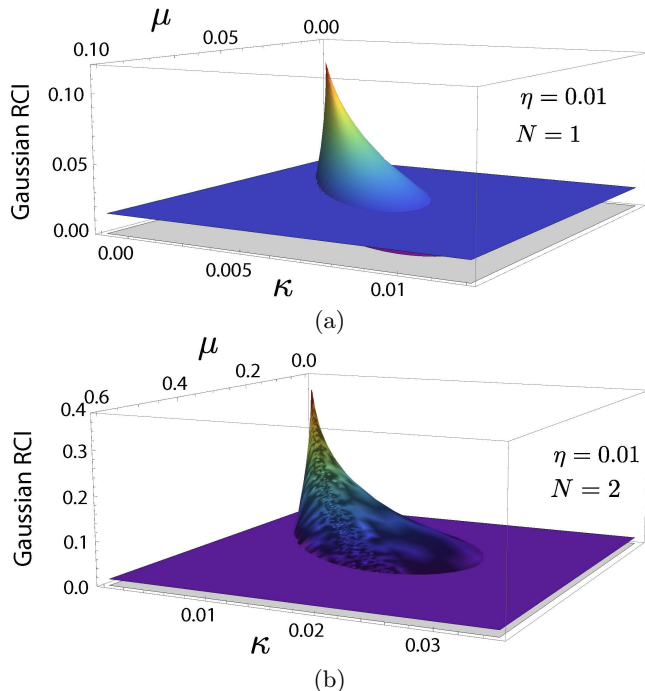


Figure 4. Gaussian RCI heralded across a pure loss channel of transmissivity $\eta = 0.01$ appended with (a) $N = 1$ -NLA, (b) $N = 2$ -NLA as a function of the input TMSV state mean photon number and the gain of the NLA. The parameter κ is related to the NLA gain by $\kappa = 1/(1 + g^2)$. The floors of the plots correspond to $C_{\text{direct}}(\eta)$. The roughness in the surface in (b) is due to the finiteness of precision in our numerics.

where $\mathbf{r} = (x_1, x_2, p_1, p_2)^T \in \mathbb{R}^4$, $\alpha = (x_1 + ip_1)/\sqrt{2}$, $\beta = (x_2 + ip_2)/\sqrt{2}$, and the Q function in real coordinates is $Q_\rho(x_1, x_2, p_1, p_2) = \langle x_1, x_2, p_1, p_2 | \rho | x_1, x_2, p_1, p_2 \rangle / (4\pi^2)$.

Given the covariance matrix $V(\rho_{AB})$ of a bipartite state ρ_{AB} , the RCI of $V(\rho_{AB})$ follows from (7) as

$$I_R(A' \langle B \rangle)_{\rho_{AB}} = H(A)_{\rho_{AB}} - H(AB)_{\rho_{AB}} = g(\vec{\nu}_A) - g(\vec{\nu}_{AB}), \quad (9)$$

where $g(x) := \left(\frac{x+1}{2}\right) \log_2 \left(\frac{x+1}{2}\right) - \left(\frac{x-1}{2}\right) \log_2 \left(\frac{x-1}{2}\right)$ is the entropy of a thermal state of mean photon number $(x-1)/2$, and $\vec{\nu}_A$ and $\vec{\nu}_{AB}$ are the symplectic eigenvalues of the covariance matrices corresponding to mode A and modes AB , respectively (Appendix A). We call this the Gaussian RCI of the state ρ_{AB} .

IV. RESULTS

A. Gaussian reverse coherent information for $N = 1, 2$ -NLA-assisted pure loss channel

In Figs. 4 and 5, we plot the Gaussian RCI and the heralding success probability for a pure loss channel appended with $N = 1$ -NLA and $N = 2$ -NLA. The quan-

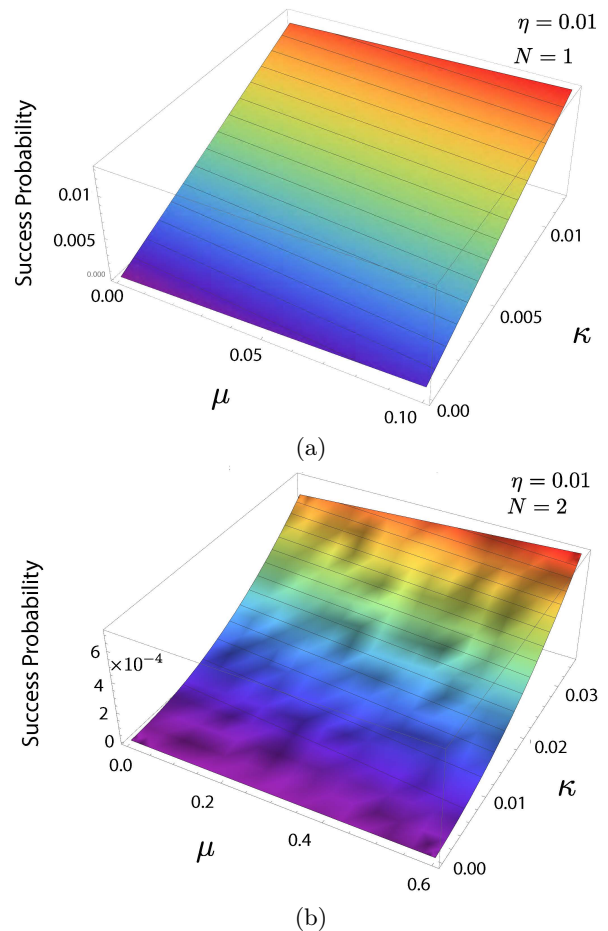


Figure 5. Heralding success probability with $N = 1, 2$ - NLA deployed on a pure loss channel of transmissivity $\eta = 0.01$, as a function of the input TMSV state mean photon number and the gain of the NLA. The parameter κ is related to the NLA gain by $\kappa = 1/(1 + g^2)$.

tity is plotted as a function of the mean photon number μ of the TMSV input and the transmissivity $\kappa = 1/(1 + g^2)$ of the asymmetric beamsplitter in the quantum scissors (g being the NLA gain). We choose a channel of transmissivity $\eta = 0.01$. The choice of a small transmissivity η for illustration is such that the amplification due to quantum scissors remains noiseless. The mean photon number of the input TMSV state is optimized to determine the best possible heralded Gaussian RCI. We make the following observations from these Figures. a) The heralded Gaussian RCI exceeds the direct transmission capacity $C_{\text{direct}}(\eta)$ of Eq. (1) (denoted by the floor of both the 3-d plots in Fig. 4) for a certain regime of the parameters μ and κ for both $N = 1, 2$. b) The Gaussian RCI of $N = 2$ -NLA is about four times that of $N = 1$ -NLA. c) The increase in the Gaussian RCI is accompanied by a steep decrease in the heralding success probability of the NLA, which drops exponentially going from $N = 1$ to $N = 2$ -NLA as shown in Fig. 5.

For a different choice of η , namely $\eta = 0.1$, the op-

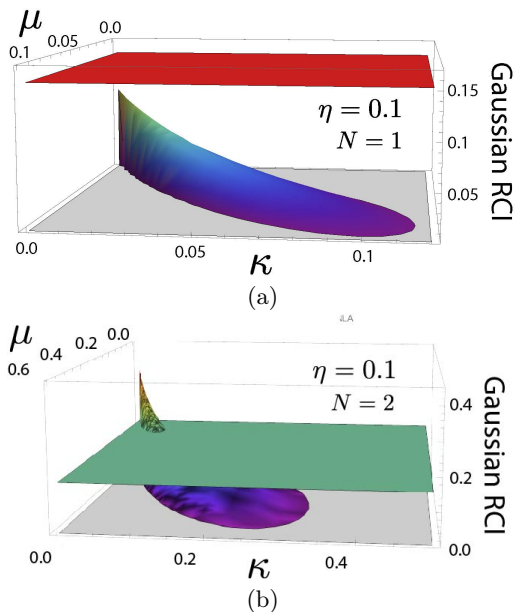


Figure 6. Gaussian RCI heralded across a pure loss channel of transmissivity $\eta = 0.1$ appended with $N = 1, 2$ -NLA, as a function of the input TMSV state mean photon number and the gain of the NLA. The parameter κ is related to the gain of the NLA by $\kappa = 1/(1 + g^2)$. The planes in the plots correspond to $C_{\text{direct}}(\eta)$.

timal heralded Gaussian RCI with $N = 1$ -NLA never exceeds $C_{\text{direct}}(\eta)$, whereas with $N = 2$ -NLA it exceeds the bound, as shown in Fig. 6. In other words, in such a parameter regime one quantum scissors is not enough, and a second quantum scissors is required to “activate” a heralded entanglement of higher quality than direct transmission.

Since the increase in the heralded Gaussian RCI happens at the expense of the decreased heralding success probability, it is important to characterize this tradeoff so that the values of the parameters (TMSV input mean photon number μ and NLA gain g) can be chosen optimally. In Fig. 7, we plot the Gaussian RCI as a function of the success probability for the $N = 1, 2$ -NLA-appended channel of transmissivity $\eta = 0.01$, when μ and g are optimized. The outer envelope of this scatter plot thus represents the best possible pairs of heralded RCI and heralding success probability attainable using $N = 1, 2$ -NLA. The oscillations in the outer envelope are a result of focusing on the Gaussian part (covariance matrix) of the heralded state, whose Q function is a sum of many Gaussian distributions and thus non-Gaussian. The envelope and the accompanying set of optimal parameters thus may be of use in designing quantum repeater schemes with quantum scissors based NLA.

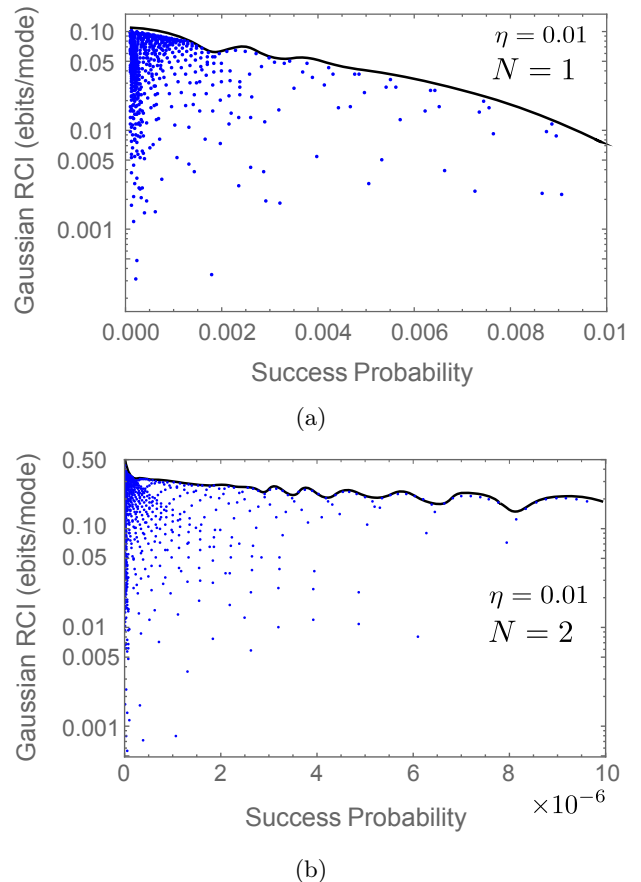


Figure 7. Gaussian RCI heralded across $N = 1, 2$ -NLA vs heralding success probability for a pure loss channel of transmissivity $\eta = 0.01$.

B. Entanglement of formation and reverse coherent information lower bounds for teleportation through NLA-assisted pure loss channel

In [34], a variant of the scheme in Fig. 2 was studied as quantum error correction for the transmission of quantum continuous variable states over a lossy channel. The scheme is as shown in Fig. 8. Here, direct transmission through the lossy channel is replaced by continuous-variable quantum teleportation over a lossy entangled resource established by sending one mode of a finite energy two-mode squeezed vacuum (TMSV) state through the channel followed by NLA. The resource is referred to as an error correction (EC) box, and is characterized by the mean photon number of the teleportation resource TMSV state μ_{res} , the number of quantum scissors N , and the NLA gain g . Using a meticulous Fock basis calculation, Dias and Ralph [33] recently showed that this scheme with $N = 1$ -NLA, when NLA is successful, can herald states with higher entanglement than the state shared via direct transmission over the lossy channel. They considered the entanglement of formation (EOF) (Appendix D) of the heralded covariance matrix

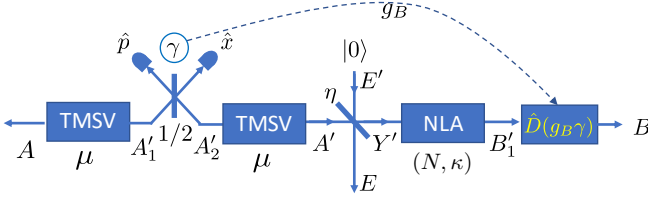


Figure 8. One mode of a TMSV state teleported through a resource state consisting of a lossy TMSV state aided by a $N = 1$ -NLA.

(Gaussian part of the heralded non-Gaussian state) as the figure of merit, which constitutes a lower bound on the entanglement of formation of the heralded non-Gaussian state by the Gaussian extremality theorem [53].

The calculation of Dias and Ralph, however, is tedious and difficult to be extended to NLA with multiple quantum scissors. The method based on characteristic functions described in Sec. III B offers an efficient alternative means to determine the heralded non-Gaussian state in this case. Using this method along with general ideas from Gaussian conditional dynamics [50, 54] to deal with the teleportation elements such as dual homodyne detection (CV Bell state measurement) and displacement (unitary correction) (Appendix B), we analyzed the effect of NLA with $N = 1, 2$ -quantum scissors in Fig. 8. We calculated a lower bound on the EOF of the heralded state by evaluating yet another measure, the Gaussian entanglement of formation (GEOF), on the Gaussian part of the heralded state, which equals its EOF. (Appendix D for details.)

In this scheme, the non-Gaussian state heralded upon successful NLA operation for a TMSV input is a function of the dual homodyne detection outcome. In particular, both its first and second moments are dependent on the outcome. There are two ways to quantify the performance of the scheme: a) evaluating the figure of merit on the covariance matrix of the average heralded state, or, b) evaluating the average of the figure of merit applied on the conditional heralded covariance matrices, where in both cases the averaging is with respect to the dual homodyne measurement outcomes. We will call these q_1 and q_2 , respectively. Operationally, the former captures the entanglement content of the average state heralded by the scheme, while the latter captures the entanglement content on a per copy basis, averaged over the copies. Convexity of the EOF implies that $q_2 \geq q_1$. It should be noted that while the displacement correction associated with the teleportation impacts the average heralded state and in turn its EOF, it does not affect the EOF of the conditional heralded states, since the measure is independent of the first moments.

In Fig. 9, we plot q_1 and q_2 for a TMSV input of mean photon number μ as a function of the effective transmission parameter defined as $\eta_{\text{effec}} = g^2 \eta \chi^2$, where g is related to the gain of the NLA, and $\chi =$

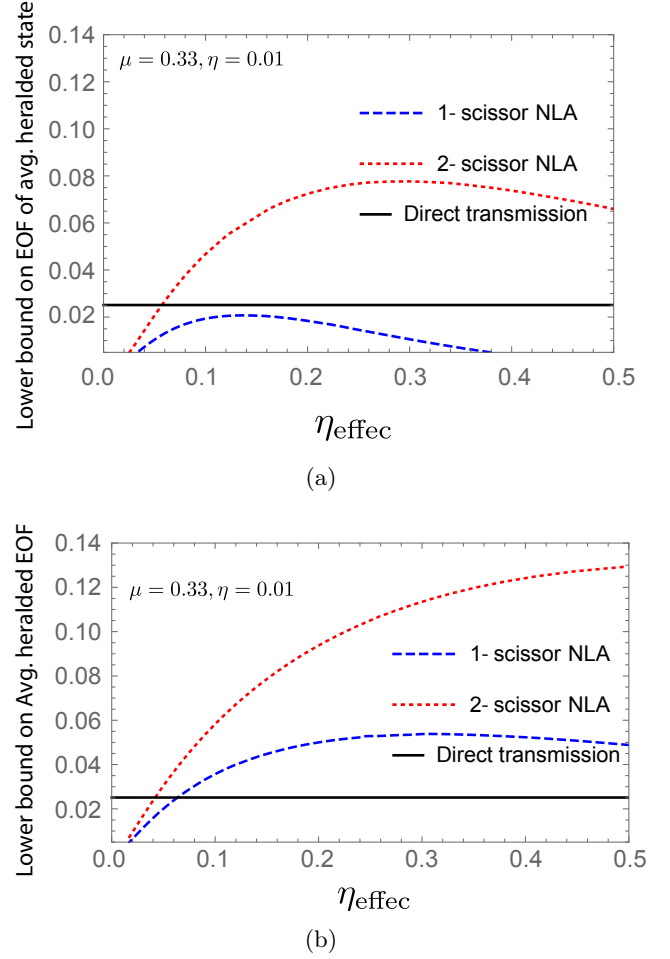


Figure 9. Entanglement of formation (EOF) of the covariance matrix heralded across the EC Box of [34] for a TMSV input, as a function of the heralded effective transmission. The bare channel transmissivity is chosen to be $\eta = 0.01$, mean photon number of the input TMSV and the teleportation resource TMSV chosen to be equal $\mu_{\text{res}} = \mu = 0.33$, $N = 1, 2$, and the NLA gain g is varied. a) The EOF of the covariance matrix of the average state heralded across the error corrected channel. b) The average of EOF of the conditional heralded covariance matrices (conditioned on and averaged over the outcome of the dual homodyne detection). The black bold line corresponds to the EOF for transmission across the bare lossy channel.

$\tanh(\sinh^{-1}(\sqrt{\mu_{\text{res}}}))$. The channel transmissivity is chosen to be $\eta = 0.01$, and the mean photon number of the TMSV state at the input as well as in the EC box (teleportation resource state) are chosen to be $\mu_{\text{res}} = \mu = 0.33$, (which corresponds to $\chi = 1$), and the NLA amplitude gain g is scanned over. In Fig. 9 (a), the quantity q_1 is plotted, where it has been optimized over a classical gain tuning parameter that scales the dual homodyne outcome prior to the displacement correction operation. We find that our curve for the $N = 1$ -NLA is qualitatively similar, but below what was reported in [33] for the same. This is as expected, since we have consid-

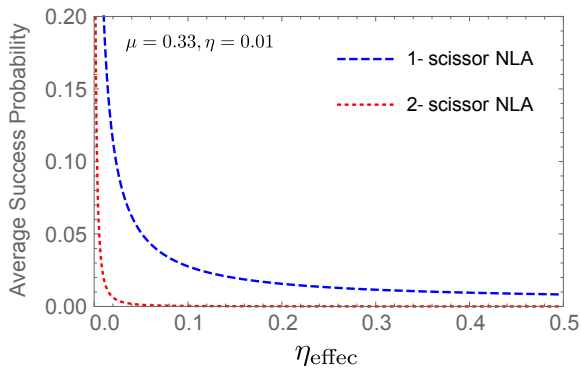


Figure 10. Success Probability of [34]’s EC box for $N = 1, 2$ -NLA as a function of the heralded effective transmission. The bare channel transmissivity is chosen to be $\eta = 0.01$, mean photon number of the input TMSV and the teleportation resource TMSV chosen to be equal $\mu_{\text{res}} = \mu = 0.33$, $N = 1, 2$, and the NLA gain g is varied.

ered ON-OFF heralding photodetection instead of perfect photon-number-resolving (PNR) single photon detection in the quantum scissors. In addition, we now have calculated the same figure of merit also for $N = 2$ -NLA. We observe that the Gaussian lower bound on the EOF of the heralded state increases significantly in going from $N = 1$ to $N = 2$. In Fig. 9 (b), the quantity q_2 is plotted, and as is expected due to convexity of the EOF, they are higher than the corresponding curves in Fig. 9 (a). In the remainder of this discussion, we will consider the quantity q_2 as the sole figure of merit for the scheme.

In Fig. 10, the heralding success probability of the scheme is plotted as a function of the effective transmission for the same set of parameter values as chosen in Fig. 9. We observe that our curve for the $N = 1$ case is qualitatively similar, but slightly above the one reported in [33]. This is again consistent with our choice of ON-OFF photodetection in place of single photon detection in the quantum scissors.

In Fig. 11, the quantity q_2 and the heralding success probability of NLA are plotted as a function of the NLA intensity gain g^2 . The EOF of direct transmission through the lossy channel forms the benchmark. This is exceeded by teleportation of the input through EC box with $N = 1, 2$ -NLA. The figure also shows the performance of ideal NLA (corresponding to $N \rightarrow \infty$) for comparison, which is calculated as the EOF of a TMSV state whose one mode undergoes a pure loss channel of effective transmissivity $\eta_{\text{effec}} = g^2 \eta \chi^2$, g being the NLA gain, and $\chi = \tanh(\sinh^{-1}(\sqrt{\mu_{\text{res}}}))$ [34].

The EOF, though a valid entanglement measure, is an upper bound on the distillable entanglement, whereas the RCI is a lower bound on the distillable entanglement, and hence more operationally relevant to entanglement distillation. We analyze the average RCI of the heralded conditional covariance matrices across the EC box. One key mathematical difference between the measures is that

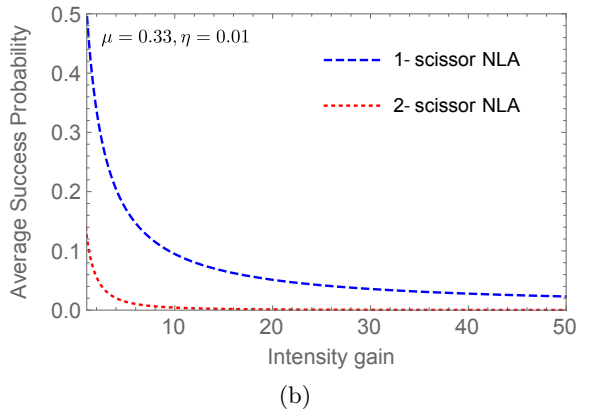
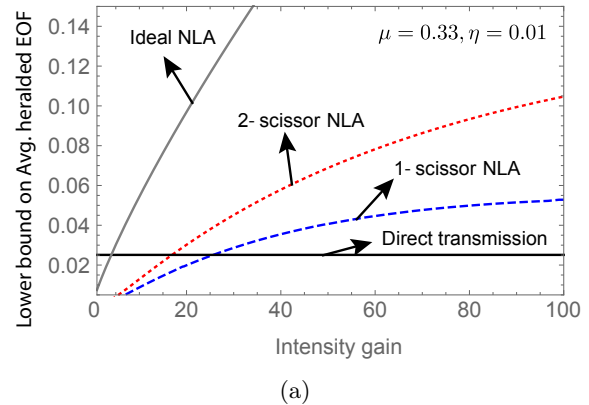


Figure 11. EOF and success probability of the covariance matrix heralded by EC box for $N = 1, 2$ -NLA as a function of the NLA intensity gain g^2 .

while the EOF is non-negative by definition, the RCI can take on negative values for separable states. We find that averaging over the dual homodyne outcomes is severely detrimental to the RCI and leaves the average RCI negative for nearly all choice of parameters. Post-selecting on the dual homodyne outcome over a small range of values around 0 (whose probability of occurrence is maximal among all possible outcomes of the measurement), we plot the average of the RCI of the heralded conditional covariance matrices in Fig. 12 for EC box with $N = 1, 2$ -NLA. These curves are identical to the ones in Fig. 4, but are attained with higher values of mean photon number μ . This is consistent with the fact that the teleportation of two TMSV heralds a new TMSV of a different mean photon number, and hence, the teleportation through the EC box converges to transmission of a different TMSV through the NLA assisted lossy channel.

V. CONCLUSIONS

To summarize, we studied continuous-variable entanglement distillation with quantum scissors-based NLA from a noisy two-mode squeezed state shared across a

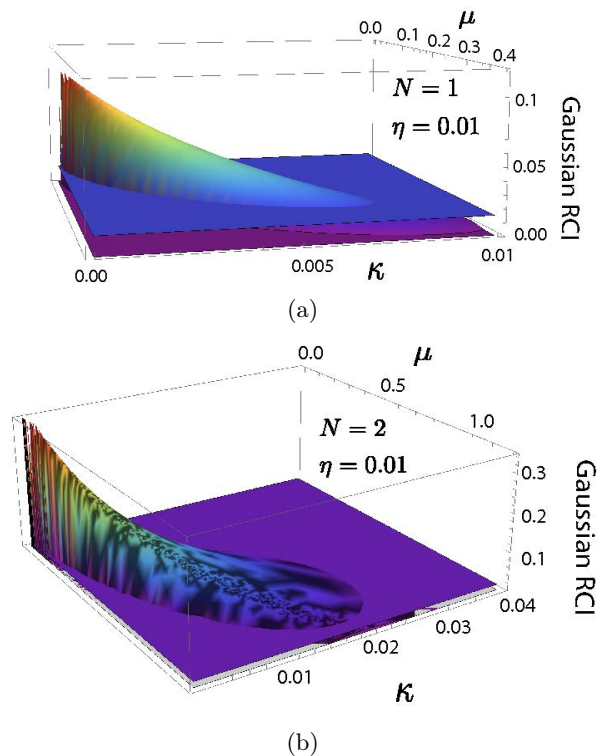


Figure 12. Reverse coherent information of the covariance matrix heralded across the scheme in Fig. 8 with $N = 1, 2$ -NLA and $\eta = 0.01$. The parameter κ is related to the gain of the NLA by $\kappa = 1/(1 + g^2)$.

pure loss channel, as shown in Figs. 2 and 3. We presented a calculation based on phase space characteristic functions and the Husimi- Q function to determine the non-Gaussian state heralded by the quantum scissors and the associated heralding probability. The complexity of the calculation scales efficiently with the number of quantum scissors. Having determined the heralded non-Gaussian state, we evaluated its Gaussian RCI and numerically optimized it over the input mean photon number and the NLA gain, where the RCI is a lower bound on the distillable entanglement per copy of the shared state when many copies are available that is achievable using one-way LOCC.

We also applied the calculation to the proposal of [34] that replaces transmission through a lossy channel with teleportation over a NLA-error corrected lossy entangled resource state as shown in Fig. 8. Previous studies on this scheme had determined the logarithmic negativity and a Gaussian lower bound on the EOF of the states heralded by single quantum scissors. We validated some of these findings with our method and extended the analysis to the case of two quantum scissors. Additionally, we calculated the Gaussian RCI for the scheme with one and two quantum scissors.

Our main conclusions include: a) In CV entanglement distillation over a pure loss channel, using the quantum

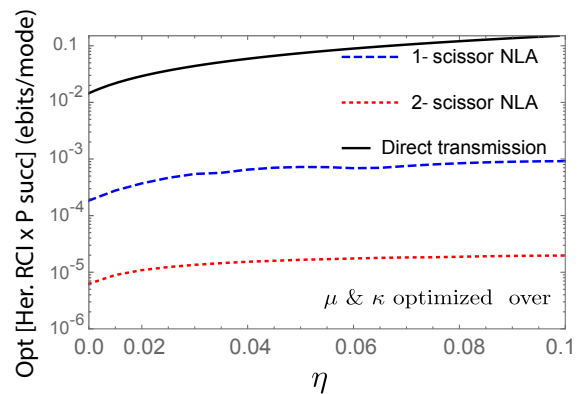


Figure 13. Numerically optimized value of the product of heralded Gaussian RCI and the heralding success probability for $N = 1, 2$ -NLA in the setup shown in Fig. 2, as a function of the pure loss channel's transmissivity η . The value is optimized over the NLA gain and the mean photon number of the input TMSV state. The black curve corresponds to the direct transmission capacity $C_{\text{direct}}(\eta) = -\log_2(1 - \eta)$.

scissors, it is possible to herald entangled states whose RCI exceeds the direct transmission entanglement distillation capacity of the channel $C_{\text{direct}}(\eta)$ of Eq. (1). b) Increasing the number of scissors amounts to higher Gaussian RCI of the heralded state. The increase in heralded Gaussian RCI comes at the expense of a significantly lower success probability. c) In some cases, a second quantum scissors can help herald a Gaussian RCI that exceeds $C_{\text{direct}}(\eta)$, while a single quantum scissors could not help exceed the bound. d) In the NLA-CV error correction scheme of Fig. 8, the Gaussian RCI heralded by the scheme, on average (over the teleportation dual homodyne detection outcomes), does not exceed $C_{\text{direct}}(\eta)$. Yet, when post-selected over a narrow window of the teleportation dual homodyne measurement outcomes around zero, it can exceed the same. In this limit of a small window of outcomes, the scheme converges to the scheme in Fig. 2—a pure loss channel appended by quantum scissors-based NLA with an entangled state input, albeit with higher optimal input mean photon numbers.

Although our results show that the quantum scissors-NLA based scheme in Fig. 3 can herald entangled states whose distillable entanglement exceeds $C_{\text{direct}}(\eta)$, they do not demonstrate a quantum repeater. In order to demonstrate a quantum repeater using the quantum scissors, the product of heralded RCI and the heralding success probability, which is the true rate of entanglement distillation, must exceed $C_{\text{direct}}(\eta)$. Clearly, as seen in Figs. 5, 7, 11 (b), the success probability of the quantum scissors drops steeply with increasing NLA gain so that the product of the heralded RCI and the heralding probability stays significantly below the direct transmission rate-loss tradeoff. This is further elucidated in Fig. 13, where the product of heralded Gaussian RCI and the heralding success probability for the setup in Fig. 3, numerically optimized over the NLA gain param-

eter and the mean photon number of the input TMSV state, is plotted as a function of channel loss for number of quantum scissors $N = 1, 2$. The curves are found to be below $C_{\text{direct}}(\eta)$, whereas the heralded RCI alone, e.g. at $\eta = 0.01$, were seen to exceed $C_{\text{direct}}(\eta)$ in Fig. 4. Nevertheless, the fact that the quantum scissors are able to herald states with distillable entanglement higher than $C_{\text{direct}}(\eta)$ paves the way towards constructing a multiplexing-based, second generation, CV quantum repeater scheme using the quantum scissors, as described in [46].

With regard to the experimental implementation of NLA using multiple quantum scissors, the primary imperfections to be considered include detection inefficiencies, single photon source inefficiencies and lack of photon number resolution. Our model for the quantum scissors in Fig. 3 already addresses the latter two considerations, while the former remains to be analyzed. The heralded RCIs and the success probability of the quantum scissors are expected to drop when detection inefficiencies are considered.

Note added- During completion of this work, we became aware of the work of [55], which investigates the use of quantum scissors-based NLA in the context of CV quantum key distribution over a thermal loss channel us-

ing a method similar to ours, and shows improved distance of transmission. They lower bound the secret key generation rate in terms of the difference of a mutual information and a Holevo information, whereas we have lower bounded the entanglement and secret key distillation rates over a pure loss channel using the reverse coherent information.

ACKNOWLEDGMENTS

KPS thanks Animesh Datta, Christos Gagatsos, Stefano Pirandola, Mark M. Wilde and Zheshe Zhang for valuable discussions. This work was supported by the Office of Naval Research program Communications and Networking with Quantum Operationally-Secure Technology for Maritime Deployment (CONQUEST), awarded under Raytheon BBN Technologies prime contract number N00014-16-C-2069, and a subcontract to University of Arizona. This document does not contain technology or technical data controlled under either the U.S. International Traffic in Arms Regulations or the U.S. Export Administration Regulations.

-
- [1] R. Van Meter and S. J. Devitt. The path to scalable distributed quantum computing. *Computer*, 49(9):31–42, Sept 2016.
 - [2] Vincent Danos, Ellie D’Hondt, Elham Kashefi, and Prakash Panangaden. Distributed measurement-based quantum computation. *Electronic Notes in Theoretical Computer Science*, 170:73 – 94, 2007. Proceedings of the 3rd International Workshop on Quantum Programming Languages (QPL 2005).
 - [3] Harry Buhrman and Hein Röhrig. Distributed quantum computing. In Branislav Rován and Peter Vojtáš, editors, *Mathematical Foundations of Computer Science 2003*, pages 1–20, Berlin, Heidelberg, 2003. Springer Berlin Heidelberg.
 - [4] Timothy J. Proctor, Paul A. Knott, and Jacob A. Dunningham. Multiparameter estimation in networked quantum sensors. *Phys. Rev. Lett.*, 120:080501, Feb 2018.
 - [5] Wenchao Ge, Kurt Jacobs, Zachary Eldredge, Alexey V. Gorshkov, and Michael Foss-Feig. Distributed quantum metrology with linear networks and separable inputs. *Phys. Rev. Lett.*, 121:043604, Jul 2018.
 - [6] Quntao Zhuang, Zheshe Zhang, and Jeffrey H. Shapiro. Distributed quantum sensing using continuous-variable multipartite entanglement. *Phys. Rev. A*, 97:032329, Mar 2018.
 - [7] Artur K. Ekert. Quantum cryptography based on bell’s theorem. *Phys. Rev. Lett.*, 67:661–663, Aug 1991.
 - [8] Charles H. Bennett, Gilles Brassard, Claude Crépeau, Richard Jozsa, Asher Peres, and William K. Wootters. Teleporting an unknown quantum state via dual classical and einstein-podolsky-rosen channels. *Phys. Rev. Lett.*, 70:1895–1899, Mar 1993.
 - [9] Charles H. Bennett and Stephen J. Wiesner. Communication via one- and two-particle operators on einstein-podolsky-rosen states. *Phys. Rev. Lett.*, 69:2881–2884, Nov 1992.
 - [10] Kenza Guenda, Somphong Jitman, and T. Aaron Gulliver. Constructions of good entanglement-assisted quantum error correcting codes. *Designs, Codes and Cryptography*, 86(1):121–136, Jan 2018.
 - [11] Charles H. Bennett, Peter W. Shor, John A. Smolin, and Ashish V. Thapliyal. Entanglement-assisted classical capacity of noisy quantum channels. *Phys. Rev. Lett.*, 83:3081–3084, Oct 1999.
 - [12] H. J. Kimble. The quantum internet. *Nature*, 453:1023, June 2008.
 - [13] Jian-Wei Pan, Zeng-Bing Chen, Chao-Yang Lu, Harald Weinfurter, Anton Zeilinger, and Marek Żukowski. Multiphoton entanglement and interferometry. *Rev. Mod. Phys.*, 84:777–838, May 2012.
 - [14] Ryszard Horodecki, Paweł Horodecki, Michał Horodecki, and Karol Horodecki. Quantum entanglement. *Rev. Mod. Phys.*, 81:865–942, Jun 2009.
 - [15] Charles H Bennett, Gilles Brassard, Sandu Popescu, Benjamin Schumacher, John A Smolin, and William K Wootters. Purification of noisy entanglement and faithful teleportation via noisy channels. *Phys. Rev. Lett.*, 76(5):722, 1996.
 - [16] David Deutsch, Artur Ekert, Richard Jozsa, Chiara Macchiavello, Sandu Popescu, and Anna Sanpera. Quantum privacy amplification and the security of quantum cryptography over noisy channels. *Phys. Rev. Lett.*, 77:2818–2821, Sep 1996.
 - [17] Jian-Wei Pan, Christoph Simon, Časlav Brukner, and

- Anton Zeilinger. Entanglement purification for quantum communication. *Nature*, 410(6832):1067–1070, 2001.
- [18] W Dür and H J Briegel. Entanglement purification and quantum error correction. *Reports on Progress in Physics*, 70(8):1381–1424, jul 2007.
- [19] J. Eisert, S. Scheel, and M. B. Plenio. Distilling gaussian states with gaussian operations is impossible. *Phys. Rev. Lett.*, 89:137903, Sep 2002.
- [20] Ryo Namiki, Oleg Gittsovich, Saikat Guha, and Norbert Lütkenhaus. Gaussian-only regenerative stations cannot act as quantum repeaters. *Phys. Rev. A*, 90:062316, Dec 2014.
- [21] Kaoru Sanaka, Kevin J. Resch, and Anton Zeilinger. Filtering out photonic fock states. *Phys. Rev. Lett.*, 96:083601, Feb 2006.
- [22] Alexander E. Ulanov, Ilya A. Fedorov, Anastasia A. Pushkina, Yury V. Kurochkin, Timothy C. Ralph, and A. I. Lvovsky. Undoing the effect of loss on quantum entanglement. *Nature Photonics*, 9:764, October 2015.
- [23] A. I. Lvovsky and J. Mlynek. Quantum-optical catalysis: Generating nonclassical states of light by means of linear optics. *Phys. Rev. Lett.*, 88:250401, Jun 2002.
- [24] Hiroki Takahashi, Jonas S Neergaard-Nielsen, Makoto Takeuchi, Masahiro Takeoka, Kazuhiro Hayasaka, Akira Furusawa, and Masahide Sasaki. Entanglement distillation from Gaussian input states. *Nature Photonics*, 4:178, feb 2010.
- [25] Animesh Datta, Lijian Zhang, Joshua Nunn, Nathan K. Langford, Alvaro Feito, Martin B. Plenio, and Ian A. Walmsley. Compact continuous-variable entanglement distillation. *Phys. Rev. Lett.*, 108:060502, Feb 2012.
- [26] Daniel E. Browne, Jens Eisert, Stefan Scheel, and Martin B. Plenio. Driving non-gaussian to gaussian states with linear optics. *Phys. Rev. A*, 67:062320, Jun 2003.
- [27] J. Eisert, D.E. Browne, S. Scheel, and M.B. Plenio. Distillation of continuous-variable entanglement with optical means. *Annals of Physics*, 311(2):431 – 458, 2004.
- [28] A. P. Lund and T. C. Ralph. Continuous-variable entanglement distillation over a general lossy channel. *Phys. Rev. A*, 80:032309, Sep 2009.
- [29] Jaromír Fiurášek. Distillation and purification of symmetric entangled gaussian states. *Phys. Rev. A*, 82:042331, Oct 2010.
- [30] T. C. Ralph and A. P. Lund. Nondeterministic noiseless linear amplification of quantum systems. *AIP Conference Proceedings*, 1110(1):155–160, 2009.
- [31] David T. Pegg, Lee S. Phillips, and Stephen M. Barnett. Optical state truncation by projection synthesis. *Phys. Rev. Lett.*, 81:1604–1606, Aug 1998.
- [32] Josephine Dias and T. C. Ralph. Quantum repeaters using continuous-variable teleportation. *Phys. Rev. A*, 95:022312, Feb 2017.
- [33] Josephine Dias and T. C. Ralph. Quantum error correction of continuous-variable states with realistic resources. *Phys. Rev. A*, 97:032335, Mar 2018.
- [34] T. C. Ralph. Quantum error correction of continuous-variable states against Gaussian noise. *Physical Review A - Atomic, Molecular, and Optical Physics*, 84(2):1–4, 2011.
- [35] William J. Munro, Koji Azuma, Kiyoshi Tamaki, and Kae Nemoto. Inside Quantum Repeaters. *IEEE Journal of Selected Topics in Quantum Electronics*, 21(3), 2015.
- [36] Nicolas Sangouard, Christoph Simon, Hugues de Riedmatten, and Nicolas Gisin. Quantum repeaters based on atomic ensembles and linear optics. *Rev. Mod. Phys.*, 83:33–80, Mar 2011.
- [37] H.-J. Briegel, W. Dür, J. I. Cirac, and P. Zoller. Quantum repeaters: The role of imperfect local operations in quantum communication. *Phys. Rev. Lett.*, 81:5932–5935, Dec 1998.
- [38] G. Y. Xiang, T. C. Ralph, A. P. Lund, N. Walk, and G. J. Pryde. Heralded noiseless linear amplification and distillation of entanglement. *Nature Photonics*, 4:316 EP –, 03 2010.
- [39] Raúl García-Patrón, Stefano Pirandola, Seth Lloyd, and Jeffrey H. Shapiro. Reverse coherent information. *Phys. Rev. Lett.*, 102:210501, May 2009.
- [40] Stefano Pirandola, Raul García-Patrón, Samuel L. Braunstein, and Seth Lloyd. Direct and reverse secret-key capacities of a quantum channel. *Phys. Rev. Lett.*, 102:050503, Feb 2009.
- [41] Igor Devetak, Marius Junge, Christopher King, and Mary Beth Ruskai. Multiplicativity of completely bounded p-norms implies a new additivity result. *Communications in Mathematical Physics*, 266(1):37–63, Aug 2006.
- [42] Michał Horodecki, Paweł Horodecki, and Ryszard Horodecki. Unified approach to quantum capacities: Towards quantum noisy coding theorem. *Phys. Rev. Lett.*, 85:433–436, Jul 2000.
- [43] Stefano Pirandola, Riccardo Laurenza, Carlo Ottaviani, and Leonardo Banchi. Fundamental limits of repeaterless quantum communications. *Nature Communications*, 8:15043, April 2017.
- [44] M. M. Wilde, M. Tomamichel, and M. Berta. Converse bounds for private communication over quantum channels. *IEEE Transactions on Information Theory*, 63(3):1792–1817, March 2017.
- [45] Igor Devetak and Andreas Winter. Distillation of secret key and entanglement from quantum states. *Proceedings of the Royal Society of London A: Mathematical, Physical and Engineering Sciences*, 461(2053):207–235, 2005.
- [46] Kaushik P. Seshadreesan, Hari Krovi, and Saikat Guha. A continuous-variable quantum repeater with quantum scissors. arXiv:1811.12393 [quant-ph].
- [47] G. Vidal and R. F. Werner. Computable measure of entanglement. *Phys. Rev. A*, 65:032314, Feb 2002.
- [48] M. B. Plenio. Logarithmic negativity: A full entanglement monotone that is not convex. *Phys. Rev. Lett.*, 95:090503, Aug 2005.
- [49] Charles H. Bennett, David P. DiVincenzo, John A. Smolin, and William K. Wootters. Mixed-state entanglement and quantum error correction. *Phys. Rev. A*, 54:3824–3851, Nov 1996.
- [50] Alessio Serafini. *Quantum Continuous Variables: A Primer of Theoretical Methods*. CRC Press, 2017.
- [51] Christian Weedbrook, Stefano Pirandola, Raúl García-Patrón, Nicolas J. Cerf, Timothy C. Ralph, Jeffrey H. Shapiro, and Seth Lloyd. Gaussian quantum information. *Rev. Mod. Phys.*, 84:621–669, May 2012.
- [52] See Supplemental Material for the code repository.
- [53] Michael M. Wolf, Geza Giedke, and J. Ignacio Cirac. Extremality of gaussian quantum states. *Phys. Rev. Lett.*, 96:080502, Mar 2006.
- [54] Marco G. Genoni, Ludovico Lami, and Alessio Serafini. Conditional and unconditional gaussian quantum dynamics. *Contemporary Physics*, 57(3):331–349, 2016.
- [55] Masoud Ghalaii, Carlo Ottaviani, Rupesh Kumar, Ste-

fano Pirandola, and Mohsen Razavi. Long-distance continuous-variable quantum key distribution with quantum scissors, 2018. arXiv:1808.01617v1.

- [56] Masahiro Takeoka, Rui-Bo Jin, and Masahide Sasaki. Full analysis of multi-photon pair effects in spontaneous parametric down conversion based photonic quantum information processing. *New Journal of Physics*, 17(4):043030, 2015.

[57] M. M. Wolf, G. Giedke, O. Krüger, R. F. Werner, and J. I. Cirac. Gaussian entanglement of formation. *Phys. Rev. A*, 69:052320, May 2004.

- [58] Paulina Marian and Tudor A. Marian. Entanglement of formation for an arbitrary two-mode gaussian state. *Phys. Rev. Lett.*, 101:220403, Nov 2008.

Appendix A: Mathematical Description of the System

Gaussian States of a Bosonic Continuous-Variable (CV) system. A system of M bosonic modes can be described by the creation and annihilation operators $\hat{a}_i^\dagger, \hat{a}_i$, such that $[\hat{a}_i, \hat{a}_j^\dagger] = \delta_{i,j}$, $[\hat{a}_i, \hat{a}_j] = [\hat{a}_i^\dagger, \hat{a}_j^\dagger] = 0 \forall i, j \in \{1, \dots, M\}$, and the corresponding quadrature operators $\hat{x}_i = (\hat{a}_i + \hat{a}_i^\dagger)/\sqrt{2}$, $\hat{p}_i = (\hat{a}_i - \hat{a}_i^\dagger)/(i\sqrt{2})$, such that $[\hat{x}_i, \hat{p}_j] = i\delta_{i,j}$.

For a quantum state $\hat{\rho}$ defined on the M -mode Hilbert space $\mathcal{H}^{\otimes M}$, a characteristic function can be defined as the following operator Fourier transform (c.f., [56])

$$\chi(\xi) = \text{Tr} \left(\hat{\rho} \hat{\mathcal{W}}(\xi) \right), \quad (\text{A1})$$

where $\hat{\mathcal{W}}(\xi)$ is the Weyl operator

$$\hat{\mathcal{W}}(\xi) = \exp(-i\xi^T \hat{\mathbf{r}}), \quad (\text{A2})$$

and $\hat{\mathbf{r}} = (\hat{x}_1, \dots, \hat{x}_M, \hat{p}_1, \dots, \hat{p}_M)^T$, $\xi = (\xi_1, \dots, \xi_{2M})^T$, $\xi_i \in \mathbb{R} \forall i \in \{1, \dots, M\}$. The characteristic function of (A1) for a quantum Gaussian state by definition is Gaussian, i.e., it can be written as

$$\chi(\xi) = \exp\left(-\frac{1}{4}\xi^T \mathbf{V} \xi - i\mathbf{s}^T \xi\right), \quad (\text{A3})$$

where \mathbf{V} is the $2M \times 2M$ real symmetric covariance matrix defined as $\mathbf{V}_{i,j} = \langle \{\hat{\mathbf{r}}_i, \hat{\mathbf{r}}_j\} \rangle_\rho - 2\langle \hat{\mathbf{r}}_i \rangle_\rho \langle \hat{\mathbf{r}}_j \rangle_\rho$ and $\mathbf{s} = \langle \hat{\mathbf{r}} \rangle_\rho$ is the $2M$ -dimensional mean displacement vector.

The vacuum state is a Gaussian state with a covariance matrix equal to the identity operator I . The two-mode squeezed vacuum (TMSV) state of mean photon number $\mu = \sinh^2(r)$ (r being the squeezing parameter) is a Gaussian state with

$$\mathbf{V}^{\text{TMSV}}(\mu) = \begin{pmatrix} \mathbf{V}^+(\mu) & 0 \\ 0 & \mathbf{V}^-(\mu) \end{pmatrix}, \quad \mathbf{V}^\pm(\mu) = \begin{pmatrix} 2\mu + 1 & \pm 2\sqrt{\mu(\mu + 1)} \\ \pm 2\sqrt{\mu(\mu + 1)} & 2\mu + 1 \end{pmatrix}, \quad (\text{A4})$$

and $\mathbf{s} = \vec{0}$. The vacuum state is a special case of the TMSV with $r = \mu = 0$.

The covariance matrix of a quantum state satisfies the Heisenberg uncertainty principle $\mathbf{V} + i\Omega \geq 0$, where

$$\Omega_n = \begin{pmatrix} 0 & 1 \\ -1 & 0 \end{pmatrix} \otimes I_{n \times n}.$$

According to Williamson's theorem, a quantum covariance matrix $\mathbf{V} + i\Omega \geq 0$ can be diagonalized as

$$\mathbf{V} = S_V (\mathbf{D}_V \oplus \mathbf{D}_V) S_V^T, \quad (\text{A5})$$

where S_V is a $2n \times 2n$ Real symplectic matrix and $\mathbf{D}_V = \text{diag}(\nu_1, \dots, \nu_n)$, where the ν_j are called the symplectic eigenvalues of \mathbf{V} .

Gaussian Unitaries. Unitary operators of the form $\hat{U}_{\mathbf{s}, S} = \exp(i\hat{H})$, where \hat{H} is a Hamiltonian that is at most quadratic in $\hat{\mathbf{r}}$ are called Gaussian unitaries. They map quantum Gaussian states into quantum Gaussian states. An arbitrary Gaussian unitary operator can be decomposed as

$$\hat{U}_{\mathbf{s}, S} = \hat{D}_{-\mathbf{s}} \hat{U}_S, \quad (\text{A6})$$

where $\mathbf{s} \in \mathbb{R}^{2M}$, $\hat{D}_{-\mathbf{s}} = \otimes_{j=1}^M \hat{D}_{-(\mathbf{s}_j, \mathbf{s}_{M+j})}$ is the displacement operator such that

$$\hat{D}_{-(\mathbf{s}_j, \mathbf{s}_{M+j})} = \exp(i(\mathbf{s}_{M+j} \hat{\mathbf{r}}_j - \mathbf{s}_j \hat{\mathbf{r}}_{M+j})), \quad (\text{A7})$$

and \hat{U}_S is a canonical Gaussian unitary operator generated by a purely quadratic Hamiltonian.

A canonical Gaussian unitary operator $\hat{U}_{\mathbf{s}, S}$ transforms the quadrature operators as

$$\hat{\mathbf{r}} \rightarrow \hat{U}_{\mathbf{s}, S} \hat{\mathbf{r}} \hat{U}_{\mathbf{s}, S}^\dagger = S \hat{\mathbf{r}} + \mathbf{s}, \quad (\text{A8})$$

where S is a $2M \times 2M$ symplectic matrix and $\mathbf{s} \in \mathbb{R}^{2M}$. Consequently, it transforms the first two statistical moments of an arbitrary quantum state as

$$\mathbf{s} \rightarrow S\mathbf{s}, \quad V \rightarrow S\mathbf{V}S^T, \quad (\text{A9})$$

where $\mathbf{s} \in \mathbb{R}^{2M}$ is the mean vector and \mathbf{V} the $2M \times 2M$ covariance matrix.

The two-mode beam splitter transformation is a canonical Gaussian unitary transformation given by

$$\hat{U}_{BS} = \exp(i\theta(\hat{x}_1 \hat{p}_2 - \hat{p}_1 \hat{x}_2)), \quad (\text{A10})$$

where $t = \cos^2 \theta \in [0, 1]$ is the transmissivity of the beamsplitter. The corresponding symplectic matrix is given by

$$S^{(t)} = \begin{pmatrix} \sqrt{t} & \sqrt{1-t} & 0 & 0 \\ -\sqrt{1-t} & \sqrt{t} & 0 & 0 \\ 0 & 0 & \sqrt{t} & \sqrt{1-t} \\ 0 & 0 & -\sqrt{1-t} & \sqrt{t} \end{pmatrix}. \quad (\text{A11})$$

Pure loss channel. The pure loss channel of transmissivity η is a Gaussian channel that maps Gaussian states to Gaussian states. It can be modeled as a beam splitter unitary transformation of the same transmissivity between the lossy mode and an environment mode that is in the vacuum state. The action of the pure loss channel on the lossy mode is obtained by tracing out the environment mode, and can be expressed as

$$\mathcal{N}^{(\eta)} : \mathbf{V} \rightarrow X^T \mathbf{V} X + Y, \quad (\text{A12})$$

where $X = \sqrt{\eta} I$ and $Y = (1 - \eta) I$.

Initial and pre-measurement state in Fig. 3. Since the pure loss channel is a Gaussian channel and the beam splitter transformation is a Gaussian unitary operation, the scheme depicted in Fig. 3, the quantum state across the five modes initially, and prior to measurements in modes A , B , C , Y , D , are both Gaussian state with zero displacement and covariance matrices given by

$$\mathbf{V}_{\text{initial}} = \mathbf{V}_{AA'}^{\text{TMSV}}(\mu) \otimes \mathbf{V}_{C'D}^{\text{TMSV}}(\mu_{aux}) \otimes I_{B'}, \quad (\text{A13})$$

$$\mathbf{V}_{\text{pre-meas}} = S_{Y', C''}^{(1/2)} S_{B', C'}^{(\kappa)} \mathcal{N}_{A' \rightarrow Y'}^\eta(\mathbf{V}_{\text{initial}}) \left(S_{B', C'}^{(\kappa)} \right)^T \left(S_{Y', C''}^{(1/2)} \right)^T, \quad (\text{A14})$$

respectively.

Appendix B: Gaussian Measurements, Conditional Dynamics and CV Teleportation

A Gaussian measurement is a projection onto a quantum Gaussian state, and thus is completely characterized by a mean vector and a covariance matrix.

Homodyne and Heterodyne Detection. Homodyne detection on a single-mode, say of the x -quadrature, is the projection on to the Gaussian state with mean vector and covariance matrix

$$\mathbf{r}_{\text{hom}} = (x_{\text{hom}}, 0)^T, \quad (\text{B1})$$

$$\mathbf{V}_{\text{hom}} = \lim_{r \rightarrow \infty} \begin{pmatrix} \exp(-2r) & 0 \\ 0 & \exp(+2r) \end{pmatrix}, \quad (\text{B2})$$

respectively, where x_{hom} is measurement outcome and $r \in \mathbb{R}$ is the squeezing parameter. Heterodyne detection, likewise, is the projection on to a coherent state with mean vector and covariance matrix, respectively being,

$$\mathbf{r}_{\text{het}} = (x_{\text{het}}, y_{\text{het}})^T, \quad \mathbf{V}_{\text{het}} = \begin{pmatrix} 1 & 0 \\ 0 & 1 \end{pmatrix}, \quad (\text{B3})$$

where $x_{het} + iy_{het} \in \mathbb{C}$ is the measurement outcome.

Dual Homodyne Detection. Dual homodyne detection is the continuous-variable analog of a Bell state measurement between two modes A and B . It is a projection of the two modes on to a displaced EPR state (displaced infinitely squeezed TMSV state, which is realized by mixing the two modes on a 50:50 beamsplitter, following by orthogonal homodyne detections on the two modes (\hat{x} measurement on one mode and \hat{p} measurement on the other). The mean vector and covariance matrix of the measurement after the beam splitter transformation of the two modes is given by

$$\mathbf{r}_{Dual-hom} = (\gamma_x, 0, 0, \gamma_y)^T, \quad (B4)$$

$$\mathbf{V}_{Dual-hom} = \lim_{r \rightarrow \infty} \begin{pmatrix} \exp(-2r) & 0 \\ 0 & \exp(-2r) \end{pmatrix} \oplus \begin{pmatrix} \exp(+2r) & 0 \\ 0 & \exp(-2r) \end{pmatrix}, \quad (B5)$$

where $\gamma_x + i\gamma_y \in \mathbb{C}$ is the measurement outcome.

Gaussian Conditional Dynamics and overlap integrals. Consider a continuous-variable system of n modes. Let AB be a bipartition of the modes such that subsystem B consists of m modes and subsystem A consists of the remaining $n - m$ modes. Let

$$\mathbf{s} = \begin{pmatrix} \mathbf{s}_A \\ \mathbf{s}_B \end{pmatrix}, \quad \mathbf{V} = \begin{pmatrix} \mathbf{V}_A & \mathbf{V}_{AB} \\ \mathbf{V}_{AB}^T & \mathbf{V}_B \end{pmatrix} \quad (B6)$$

be the mean vector and covariance matrix of a quantum Gaussian state $\hat{\rho}$ over the systems A and B . The quantum state obtained in mode A by tracing out subsystem B , namely $\hat{\rho}_A = \text{Tr}_B(\rho_{AB})$ is also a quantum Gaussian state with mean vector and covariance matrix given by

$$\mathbf{s} = \mathbf{s}_A, \quad \mathbf{V} = \mathbf{V}_A, \quad (B7)$$

respectively. On the other hand, when the subsystem B is measured by a Gaussian projective operator $\hat{\rho}^G$ of mean vector $\mathbf{r}_m \in \mathbb{R}^{2m}$ and covariance matrix \mathbf{V}_m , then the quantum state $\hat{\rho}_A$ conditioned on the measurement outcome $\mathbf{r}_m \in \mathbb{R}^{2m}$ is a quantum Gaussian state too, but its mean vector and covariance matrix are given by [50, 54]

$$\begin{aligned} \mathbf{s} &= \mathbf{s}_A + \mathbf{V}_{AB} \frac{1}{\mathbf{V}_B + \mathbf{V}_m} (\mathbf{r}_m - \mathbf{s}_B), \\ \mathbf{V} &= \mathbf{V}_A - \mathbf{V}_{AB} \frac{1}{\mathbf{V}_B + \mathbf{V}_m} \mathbf{V}_{AB}^T, \end{aligned} \quad (B8)$$

where the probability density function of the outcome \mathbf{r}_m is given by the Gaussian overlap integral $p(\mathbf{r}_m) = \text{Tr}(\hat{\rho}_B^G \hat{\rho}_{AB})$, which evaluates to

$$p(\mathbf{r}_m) = \frac{\exp\left(-(\mathbf{r}_m - \mathbf{s}_B)^T \frac{1}{\mathbf{V}_B + \mathbf{V}_m} (\mathbf{r}_m - \mathbf{s}_B)\right)}{\pi^m \sqrt{\det(\mathbf{V}_B + \mathbf{V}_m)}}. \quad (B9)$$

CV Teleportation of a TMSV across the EC Box of [34]. Consider the scheme in Fig. 8. Since the dual homodyne detection, the lossy channel, and the beamsplitters in the quantum scissors are all Gaussian operations, the joint quantum state across the modes prior to the measurements in the quantum scissors is Gaussian. The mean and covariance matrix of this Gaussian can be written down using (A4), (A11), (A12) and (B8).

Based on the observed dual homodyne outcome γ , after the NLA operation, a displacement correction unitary is applied on the modes A and B , where these modes are displaced back by $g_A(-\gamma_x, -\gamma_y)$ and $g_B(-\gamma_x, +\gamma_y)$. Here g_A, g_B are classical gain parameters, which can be optimized over.

Appendix C: Non-Gaussian Measurement based on ON-OFF Photodetection & Gaussian Overlap Integrals

ON-OFF photodetection is a measurement scheme described by the positive operator valued measure (POVM) elements

$$\Pi_0 = |0\rangle\langle 0|, \quad \Pi_1 = I - \Pi_0, \quad (C1)$$

where the projective measurement Π_0 is Gaussian, but Π_1 is not. In the modified quantum scissors operation considered in this work, both in Figs. 3, 8, the heralding measurements of NLA are based on ON-OFF photodetection.

When the subsystem B consisting of m out of n modes of a CV system AB in a quantum Gaussian state $\hat{\rho}_{AB}$ is measured with OFF photodetection (Π_0 projection) on all the m modes, the conditional (Gaussian) quantum state on subsystem A and the probability of obtaining the OFF outcome across the m modes follow from (B8) and (B9), respectively, with $\mathbf{V}_m = I^{\otimes m}$ and $\mathbf{r}_m = 0$. The latter is the overlap integral $\text{Tr}(\Pi_0 \hat{\rho})$, and simplifies to

$$p_{\bar{0}} = \text{Tr}((\Pi_0^{\otimes m})_B \hat{\rho}_{AB}) = \frac{2^m \exp\left(-\mathbf{s}_B^T \frac{1}{\mathbf{V}_B + I^{\otimes m}} \mathbf{s}_B\right)}{\sqrt{\det(\mathbf{V}_B + I^{\otimes m})}}, \quad (\text{C2})$$

where \mathbf{s}_B and \mathbf{V}_B are the mean and covariance matrix of the modes in B .

Likewise, the probability of observing Π_1 on all the m modes is given by

$$p_{\bar{1}} = \text{Tr}((\Pi_1^{\otimes m})_B \hat{\rho}_{AB}) \quad (\text{C3})$$

$$= \text{Tr}((\Pi_1^{\otimes m})_B \hat{\rho}_B) \quad (\text{C4})$$

$$= \text{Tr}\left((\mathbb{I} - \Pi_0)_B^{\otimes m} \hat{\rho}_B\right) \quad (\text{C5})$$

$$= \sum_{\tau \in \mathcal{P}(\mathcal{K})} (-1)^{|\tau|} \frac{2^{|\tau|} \exp\left(-\mathbf{s}_\tau^T \frac{1}{\mathbf{V}_\tau + I_{|\tau|}} \mathbf{s}_\tau\right)}{\sqrt{\det(\mathbf{V}_\tau + I_{|\tau|})}}, \quad (\text{C6})$$

where \mathcal{K} is the set of all m modes contained in system B , $\mathcal{P}(\mathcal{K})$ the powerset of \mathcal{K} , i.e., the set of all subsets of \mathcal{K} (inclusive of the null element), \mathbf{s}_τ and \mathbf{V}_τ are the mean vector and covariance matrix of the reduced quantum state on the modes in element $\tau \in \mathcal{P}(\mathcal{K})$ and $I_{|\tau|}$ is the identity matrix of dimension $|\tau|$. Though, in this case the post measurement state on subsystem A is non-Gaussian, and hence cannot be captured using (B8) anymore. Nevertheless, the Husimi Q function of the non-Gaussian state on the modes in subsystem A can be written down, e.g., when A consists of two modes \hat{a}, \hat{b} , as

$$Q(\alpha, \beta) = \frac{\text{Tr}(|\alpha\rangle\langle\alpha|_a \otimes |\beta\rangle\langle\beta|_b \otimes (\Pi_1^{\otimes m})_B \hat{\rho}_{AB})}{\pi^2 p_{\bar{1}}} \quad (\text{C7})$$

$$\Rightarrow Q(\alpha_x, \beta_x, \alpha_y, \beta_y) = \frac{\sum_{\tau \in \mathcal{P}(\mathcal{K})} (-1)^{|\tau|} \frac{2^{2|\tau|+2} \exp\left(-(\mathbf{s}_{\tau \cup A} - \mathbf{r}_{\tau \cup A})^T \frac{1}{\mathbf{V}_{\tau \cup A} + I_{|\tau|+2}} (\mathbf{s}_{\tau \cup A} - \mathbf{r}_{\tau \cup A})\right)}{\sqrt{\det(\mathbf{V}_{\tau \cup A} + I_{|\tau|+2})}}}{4\pi^2 p_{\bar{1}}}, \quad (\text{C8})$$

where $\alpha = (\alpha_x + i\alpha_y)/\sqrt{2}$ (and likewise β), and $\mathbf{r}_{\tau \cup A}$ is the zero vector except for the entries corresponding to the modes in A , which take the values $(\alpha_x, \beta_x, \alpha_y, \beta_y)$.

The same approach can be used to construct the Q function that is heralded when some of the modes in B are projected onto Π_0 , while some others are projected onto Π_1 , which is how we construct the Q function heralded by the N -quantum scissors NLA operations.

Appendix D: Entanglement of Formation

Definition 1. The entanglement of formation (EOF) of a bipartite state ρ_{AB} is defined as [49]

$$E_F(\rho_{AB}) := \inf \left\{ \sum_k \lambda_k E(|\Psi_k\rangle) \mid \rho_{AB} = \sum_k \lambda_k |\Psi_k\rangle\langle\Psi_k| \right\}, \quad (\text{D1})$$

where $|\Psi_k\rangle$ are entangled pure states and $E(|\Psi_k\rangle)$ is the entanglement entropy of $|\Psi_k\rangle$.

It is the minimum amount of pure entanglement required to construct the state ρ_{AB} . The EoF is non-increasing under local operations and classical communication (LOCC).

Definition 2. The Gaussian entanglement of formation (GEOF) of a bipartite state ρ_{AB} of mean vector d and $4n \times 4n$ dimensional covariance matrix V ($2n$ total modes) is defined as [57]

$$E_G(\rho_{AB}(V, d)) := \inf_{\lambda} \left\{ \int \lambda(dV_p, d\xi) E(\Psi_{AB}^G(V_p, \xi)) \mid \rho_{AB} = \int \lambda(dV_p, d\xi) \Psi_{AB}^G(V_p, \xi) \right\}, \quad (\text{D2})$$

$$\begin{array}{c}
\textcircled{1} E_F(\tau) \geq E_F(\tau^G) \\
\textcircled{3} \wedge \quad \textcircled{4} \quad \parallel \quad \textcircled{5} \\
E_G(\tau) \geq E_G(\tau^G) \\
\textcircled{2}
\end{array}$$

Figure 14. Relation between entanglement of formation and Gaussian entanglement of formation. τ represents a bipartite non-Gaussian state, while τ^G denotes a Gaussian state whose covariance matrix is the same as that of τ . The numberings correspond to the numberings of the text in Appendix D.

where Ψ_{AB}^G are entangled Gaussian pure states and λ is a measure in probability space. For a $n|n$ -mode bipartite state (total $2n$ modes), the GEoF is given by

$$E_G(\rho_{AB}(V, d)) = \sum_{k=1}^n H(r_k), \quad (\text{D3})$$

$$H(r) = \cosh^2(r) \log_2(\cosh^2(r)) - \sinh^2(r) \log_2(\sinh^2(r)). \quad (\text{D4})$$

This is so because every $n|n$ -mode bipartite pure Gaussian state is a tensor product of n two mode squeezed states with squeezing parameters r_k , $k \in \{1, \dots, n\}$ up to a local GLOCC unitary operation, and the entanglement of a TMS state with squeezing r is $H(r)$ as above.

It is the minimum amount of pure Gaussian entanglement required to construct the state ρ_{AB} . The GEOF is non-increasing under Gaussian local operations and classical communication (GLOCC).

Corollary 3. *The Gaussian entanglement of formation is at least as large as the entanglement of formation*

$$E_G(\rho_{AB}) \geq E_F(\rho_{AB}). \quad (\text{D5})$$

Proof. This follows from Definitions 2 and 1. The former is an infimum over a restricted set of possible decompositions of the state than the latter, and hence is equal or larger than the latter. \square

Lemma 4. *(Gaussian extremality of EOF and GEOF) Among the set of all quantum states with covariance matrix V , and arbitrary mean and other moments, the (Gaussian) entanglement of formation is minimized by the Gaussian states whose covariance matrix equals V , i.e.,*

$$E_{F/G}(\rho_{AB}(V)) \geq E_{F/G}(\rho_{AB}^G(V)). \quad (\text{D6})$$

Proposition 5. *For any two-mode Gaussian state ρ_{AB}^G , the Gaussian entanglement of formation equals its entanglement of formation, i.e.,*

$$E_G(\rho_{AB}^G) = E_F(\rho_{AB}^G). \quad (\text{D7})$$

Proof. See [58]. \square

Lemma 6. *The Gaussian entanglement of formation of a bipartite Gaussian state of mean d and covariance matrix V equals*

$$E_G(\rho_{AB}^G(V, d)) := \inf_{V_p} \{E(\rho_{AB}^G(V_p, 0)) \mid V_p \leq V\}, \quad (\text{D8})$$

where $\rho_{AB}^G(V_p, 0)$ are pure entangled states, and E is the entanglement entropy.

Proof. See [57, 58]. We use the results in [58] to evaluate the (Gaussian) entanglement of formation of the heralded covariance matrix in the NLA-assisted communication schemes. \square

Remark 7. Evidently, from Lemma 6, the Gaussian entanglement of formation is independent of displacements and equals the entanglement entropy of a TMSV state, wherein the infimum picks the TMSV state with the smallest possible squeezing.

Corollary 8. *When the covariance matrix of a non-Gaussian quantum state ρ_{AB} is $V(\gamma)$, where γ is some complex parameter distributed according to $P(\gamma)$, we have that*

$$\int d\gamma P(\gamma) E_{F/G}(\rho_{AB}(V(\gamma))) \geq \int d\gamma P(\gamma) E_{F/G}(\rho_{AB}^G(V(\gamma))). \quad (\text{D9})$$

Proof. This follows from Lemma 4 and the fact that $P(\gamma) \geq 0$ and $E_{F/G} \geq 0$ for any state. \square

Remark 9. We use the lower bound in Corollary 8 (with E_G) as our figure of merit for the scheme depicted in Fig. 8.

Remark 10. A deterministic displacement operation affects only the mean of a generic quantum state, and doesn't change its covariance matrix or higher moments.

Corollary 11. *Given a generic conditional state $\rho_{AB}(\gamma)$ of mean $d(\gamma)$ and covariance matrix $V(\gamma)$, conditioned on a parameter γ (e.g., γ could be the outcome of a dual homodyne detection), the action of conditional displacements $D(g\gamma)$ on the state doesn't change its GEOF or the average GEOF of Corollary (8).*

Remark 12. Thus, teleportation displacement correction does not affect the ergodic average GEOF lower bound we calculate for Ralph's scheme.
